Inception-Powered Unrolling Reconstruction for Accelerated Dynamic Cardiac Late Gadolinium Enhancement MRI

Ya Zhong[1,2⋆], Jing Cheng[2], Pan Wang[3], Zhaonan Zhang[4], Lixin Du[3], Weixiong Fan[4], Xin Liu[2], Dong Liang[2], Yuanyuan Liu[2⋆⋆], and Yanjie Zhu[2]

[1] Chongqing University of Technology
[2] Paul C. Lauterbur Research Center for Biomedical Imaging, Shenzhen Institutes of Advanced Technology, Chinese Academy of Sciences, Shenzhen, China
[3] Shenzhen Longhua District Central Hospital, Shenzhen, China
[4] Meizhou People's Hospital, Guangdong, Meizhou, China

Abstract. Late Gadolinium Enhancement (LGE) is the gold standard for myocardial scar assessment, yet conventional static LGE acquisition is prone to artifacts from respiratory and cardiac motion. We reinterpret LGE imaging as a highly accelerated dynamic multi-frame reconstruction problem. By partitioning sequential k-space acquisition into multiple temporal frames without extending scan time, we reconstruct these frames independently to improve motion robustness. To enable reliable reconstruction under extreme undersampling, we develop an inception-powered physics-guided unrolling method. The multi-branch inception design expands the receptive field per iteration, facilitating the separation of structured aliasing from fine myocardial details. Additionally, a parameter-shared fixed-point implementation reduces memory consumption. Experiments on large-scale clinical 3T (100 patients) and 5T datasets demonstrate consistent improvements over state-of-the-art baselines. Notably, even under challenging free-breathing conditions, our method robustly reconstructs high-quality images, demonstrating strong potential for clinical diagnostics.

Keywords: Dynamic cardiac MR · Late Gadolinium Enhancement (LGE) · Deep Unrolling Network · Image Reconstruction.

1 Introduction

Myocardial scar assessment via Late Gadolinium Enhancement (LGE) is essential for clinical diagnostics [5]. Frame-Sensitive Inversion Recovery (PSIR) [11] is widely utilized in this context due to its robustness to inversion time variability. However, conventional LGE relies on static acquisition at a single cardiac frame, which cannot capture dynamic cardiac motion or functional information.

⋆ Y. Zhong and J. Cheng contributed equally to this work.
⋆⋆ Corresponding authors: Y. Liu and Y. Zhu.

Therefore, dynamic LGE reconstruction is required to better acquire such dynamic information. Existing studies have explored two main directions to address this limitation. Motion-corrected LGE methods reduce motion-related artifacts through motion estimation and compensation, but their performance can depend on the accuracy of motion estimation [14, 26, 7]. Another approach relies on rapid imaging techniques to freeze the cardiac motion states, but maintaining image quality under high acceleration remains challenging [23, 16]. To achieve dynamic multi-frame reconstruction without extending scan time, the acquired k-space data must be distributed across multiple temporal frames, making each frame highly undersampled and substantially increasing reconstruction difficulty. In clinical practice, compressed sensing (CS) relies on hand-crafted sparsity priors and iterative solvers, often producing residual artifacts at high acceleration rates and typically limiting practical acceleration to below five-fold [13, 6]. Deep Unrolling (DU) networks [9, 3, 22] improve reconstruction by integrating model-based optimization with learned regularization. Nevertheless, most existing DU frameworks employ standard convolutional architectures with limited receptive fields [21]. When applied to high-dimensional dynamic sequences, they struggle to model complex spatiotemporal correlations [18], particularly under extreme undersampling where severe aliasing artifacts obscure fine cardiac structures. To address these challenges, we design a highly accelerated dynamic LGE reconstruction strategy and propose IPUR-LGE, an Inception-powered unrolling framework for accelerated dynamic cardiac LGE reconstruction. Inception-based multi-branch operators are incorporated within each unrolled iteration to increase receptive field diversity and enhance multi-scale feature modeling [25]. In addition, a parameter-sharing fixed-point formulation is adopted to improve memory efficiency and computational scalability in dynamic reconstruction [2, 27]. Our main contributions are as follows:

1. We reformulate segmented PSIR-LGE reconstruction as a dynamic multi-frame reconstruction problem that preserves temporal information from sequential acquisitions, improving motion robustness without extending acquisition time.
2. We introduce an inception-powered deep unrolling framework that enhances multi-scale representation within iterative reconstruction.
3. We validate the proposed framework on large-scale 3T clinical data (100 subjects) and additional 5T data, demonstrating consistent improvements over existing reconstruction baselines.

2 Method

2.1 Forward model for LGE image reconstruction

To formulate LGE reconstruction as a dynamic multi-frame inverse problem, sequential segmented k-space data [17] are partitioned into multiple frames according to the acquisition order, transforming the reconstruction target into a dynamic image sequence $x \in \mathbb{C}^{N \times T}$, where T denotes the number of frames and

N denotes the number of voxels. The forward acquisition process is formulated as $y = Ex + n$, where $y \in \mathbb{C}^M (M \ll N)$ represents the acquired undersampled k-space data, n is additive system noise, and $E = PFS$ is the encoding operator comprising undersampling mask P, Fourier transform F, and sensitivity map S. To recover x, we solve the regularized optimization problem:

$$\min_x \frac{1}{2}\|Ex - y\|_2^2 + \mathcal{R}(x) \tag{1}$$

where $\frac{1}{2}\|Ex - y\|_2^2$ denotes the data fidelity term, $\mathcal{R}(x)$ is a regularization term that imposes prior knowledge on the image x. Rather than relying on handcrafted priors such as temporal sparsity used in traditional compressed sensing (CS), we implicitly parameterize $\mathcal{R}(x)$ through a learnable operator to capture the complex spatiotemporal correlations of continuous physiological motion.

2.2 Deep Unrolling Proximal Gradient Framework

To solve the aforementioned optimization problem and capture the complex spatiotemporal correlations inherent in dynamic LGE image sequences, we propose the IPUR-LGE method (Fig. 1), which unrolls the Proximal Gradient Descent (PGD) algorithm into a deep proximal gradient method [15]. Each iteration (n=1, ..., N) alternately solves two subproblems to refine the reconstruction:

(a) Data Consistency (DC) Subproblem:

$$\mathrm{V_n} = x_{n-1} - \eta E^H \left(Ex_{n-1} - y\right) \tag{2}$$

This step employs a learnable step size η to ensure data fidelity by calculating the residual between the current x_{n-1} and the original k-space data y.

(b) Regularization (R) Subproblem:

$$x_n = \Gamma_\theta \left(\mathrm{V_n}\right) \tag{3}$$

This step uses a learnable regularizer Γ_θ to perform denoising and detail recovery on $\mathrm{V_n}$, yielding the refined output x_n. To address memory constraints, we formulate this unrolled process as a weight-shared equilibrium model [2, 12]. This iteration can be viewed as an implicit function $x_n = f_\theta \left(x_{n-1}; y\right)$, which aims to find a fixed point x^*. Through N iterations, the network is driven to approximate an equilibrium state, thereby enhancing its expressiveness and stability.

To parameterize Γ_θ for the highly complex spatiotemporal distributions of cardiac motion, we employ the network with inception modules. Unlike standard Convolutional Neural Networks with fixed receptive fields, the parallel multi-branch inception operator adaptively expands the effective receptive field, successfully preserving both global dynamic boundaries and local fine cardiac details. The framework is initialized with a coil-combined adjoint reconstruction $\left(x_0 = E^H y\right)$ using sensitivity maps pre-calibrated by the ESPIRiT method [20]. The overall framework is shown in Fig.1.

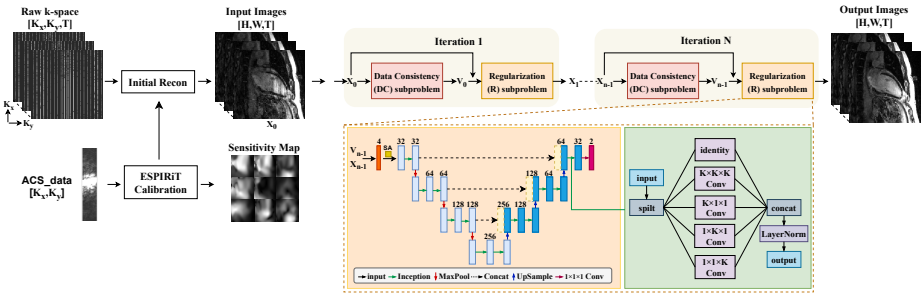

Fig. 1. Overall IPUR-LGE framework. An initial reconstruction enters an N-stage unrolling loop, which alternates two subproblems: Data Consistency (DC) and Regularization (R). The R module employs a U-Net architecture integrating Spatial Attention (SA) and Inception blocks. By processing inputs via parallel multi-kernel convolutions and an identity map, it iteratively refines features to yield high-quality images.

2.3 Final Frame-Sensitive Inversion Recovery Reconstruction

In this study, we utilize the PSIR technique for LGE imaging, in which the raw data consists of two parts: (1) Inversion Recovery image data (x_{IR}) that capture the T1-weighted contrast of infarcted myocardium, (2) reference image data (x_{Ref}) acquired with fully recovered magnetization to serve as a background frame reference. After reconstructing x_{IR} and x_{Ref} separately, the final PSIR reconstruction can be calculated using the following equation [24][11]:

$$\begin{cases} \varphi\left(x_{Ref}\right) = \arctan\left(x_{Ref}\right) \\ Z_{\text{real}} = \text{real}\left(x_{IR} \cdot e^{-i \cdot \varphi\left(x_{Ref}\right)}\right) \end{cases} \tag{4}$$

where $\varphi\left(x_{Ref}\right)$ is the background frame extracted from the reference image, and Z_{real} is the final reconstructed PSIR image.

3 Experiments

3.1 Datasets and Implementation Details

1. **Training Data:** Due to the lack of fully-sampled dynamic LGE ground truth, we used a mixed-modality training set of 3,923 slices (2866 Cine, 742 LGE, 97 Perfusion, 218 T1-weighted) from the public CMRxRecon dataset[5].Although the original LGE and T1-weighted images are inherently static, we simulated them into dynamic data by introducing noise.
2. **Clinical Testing Data and Acquisition:** Evaluation was performed on two independent clinical datasets: the 3T dataset (100 subjects, 1,184 slices, uMR890, United Imaging) and the 5T dataset (7 subjects, 144 slices, uMR-Jupiter, United Imaging). The clinical data were acquired using segmented

[5] https://github.com/CmrxRecon/CMRxRecon2025

PSIR-LGE sequences. In our reconstruction, sequential k-space segments acquired across adjacent R-R intervals were organized into 5–8 reconstructed frames depending on the acquisition orientation. A time-interleaved Cartesian undersampling strategy was used for both the 3T and 5T datasets. Due to subject-specific protocol adjustments, the field of view ranged from 280–350 mm for 3T and 290–350 mm for 5T, with an in-plane spatial resolution of approximately 1.3–1.5 mm. Typical TR/TE values were 4.3/1.82, 5.2/2.13, and 4.2/1.73 ms for 4CH, 3CH/2CH, and SAX, respectively.

3. **Implementation details:** IPUR-LGE was implemented in PyTorch and trained for 150 epochs on four NVIDIA RTX 5880 GPUs using the ADAM optimizer (learning rate 1e-4, batch size 1/GPU). A dynamic Cartesian undersampling strategy with acceleration factors (R) ranging from 4 to 16 was employed during training [19]. The model was optimized using a combined MAE and perceptual loss with equal weighting.

3.2 Experimental Design and Evaluation Metrics

To comprehensively evaluate IPUR-LGE, experiments were conducted in four aspects:

1. **Comparative Experiments:** IPUR-LGE was compared with Compressed Sensing (CS) [13] and three classical deep unrolling reconstruction methods including L+S-Net [10], Learned_DC [4], and MoDL [1]. As fully-sampled data are unavailable in clinical settings, GRAPPA reconstruction [8] with $R = 2$ is adopted as the reference.
2. **Ablation Studies:** Ablation studies validated the contributions of the inception module and the mixed-data training strategy by comparing the complete architecture with a w/o inception variant and a w/o LGE model.
3. **Noise Robustness Analysis:** To evaluate stability under challenging conditions, synthetic noise with signal-to-noise ratio (SNR) ranging from 10 dB to 30 dB was independently added to each coil channel in the image domain. Performance was compared between IPUR-LGE and L+S-Net.
4. **Motion Robustness Analysis:** We validated the clinical feasibility against standard single-frame static LGE imaging, including evaluations under free-breathing conditions to demonstrate motion-artifact mitigation.

Reconstruction performance was quantitatively evaluated using Peak Signal-to-Noise Ratio (PSNR), Structural Similarity Index (SSIM), and Root Mean Squared Error (RMSE).

4 Results

Fig. 2 shows multi-frame reconstructions of myocardial infarction patients on 3T and 5T datasets with different comparison methods. The CS method exhibited noticeable structural blurring and severe aliasing artifacts. The deep unrolling method, Learned_DC, failed to effectively remove undersampling interference,

Table 1. Average quantitative performance (PSNR, SSIM, RMSE) of different reconstruction methods on the 3T and 5T datasets across all standard views.

		PSNR	SSIM	RMSE
3T	**IPUR-LGE**	**39.2 ± 2.6**	**0.9568 ± 0.0198**	**0.0142 ± 0.0055**
	L+S-Net	36.0 ± 3.2	0.9105 ± 0.0542	0.0171 ± 0.0068
	Learned_DC	34.5 ± 3.1	0.8984 ± 0.0389	0.0203 ± 0.0071
	MoDL	32.9 ± 3.3	0.7457 ± 0.1002	0.0242 ± 0.0092
	CS	30.4 ± 3.2	0.7227 ± 0.1282	0.0325 ± 0.0115
5T	**IPUR-LGE**	**36.9 ± 4.1**	**0.9231 ± 0.0112**	**0.0195 ± 0.0059**
	L+S-Net	34.8 ± 2.1	0.8998 ± 0.0174	0.0214 ± 0.0044
	Learned_DC	32.5 ± 2.4	0.8801 ± 0.0252	0.0236 ± 0.0067
	MoDL	31.2 ± 2.3	0.7817 ± 0.0308	0.0256 ± 0.0072
	CS	30.1 ± 2.3	0.7267 ± 0.0346	0.0294 ± 0.0075

resulting in obvious residual artifacts and loss of image details. While MoDL contained obvious noise, L+S-Net performed slightly better visually but still lacked structural details. In contrast, IPUR-LGE effectively suppressed artifacts and accurately preserved fine boundaries between hyper-enhanced scars and healthy myocardium. Quantitative results in Table 1 corroborate these visual advantages, with IPUR-LGE achieving the best index across both datasets.

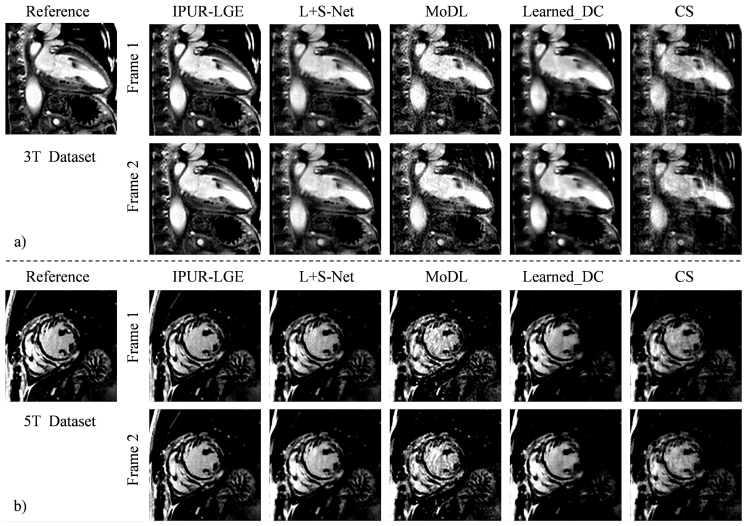

Fig. 2. Reconstruction performance comparison. (a) 3T data ($R = 14.8$) from a 65-year-old male with Myocardial Infarction with Non-Obstructive Coronary Arteries. (b) 5T data ($R = 12.5$) from a 31-year-old male with myocardial infarction.

Fig.3 shows the results of ablations under different configurations. The w/o inception model exhibited over-smoothed myocardial textures, and the w/o LGE model misinterpreted LGE-specific signal fluctuations as noise, producing a static effect lacking continuous cardiac motion. The y-t plots on the right side further

confirm this observation. Both ablated methods present temporal frame-induced discontinuities, as indicated by the yellow arrows. IPUR-LGE successfully corrected these domain biases. Quantitative analysis in Table 2 confirms these advantages across all anatomical views, demonstrating the necessity of the Inception module and mixed-data strategy.

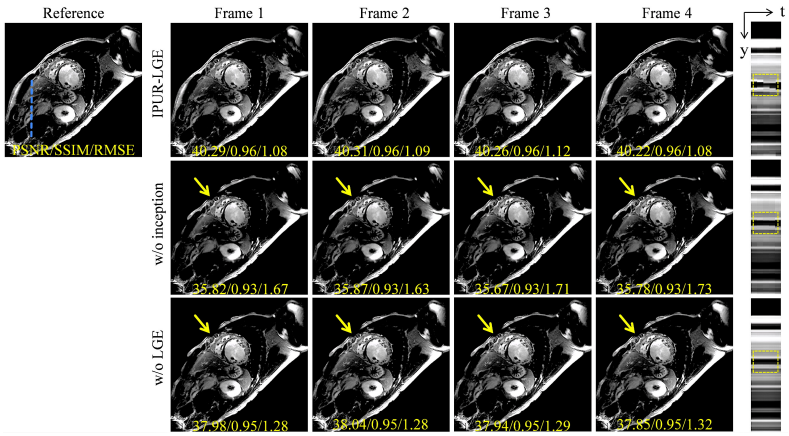

Fig. 3. Ablation results from a 69-year-old male patient. Yellow arrows indicate inter-frame structural inconsistencies in the ablated variants. A vertical blue dashed line on the reference image marks the spatial location used for the y–t plots (rightmost column). Yellow boxes highlight that IPUR-LGE better preserves structural consistency across reconstructed frames compared with the w/o inception and w/o LGE variants. Metrics are PSNR/SSIM/RMSE, with RMSE scaled by 100.

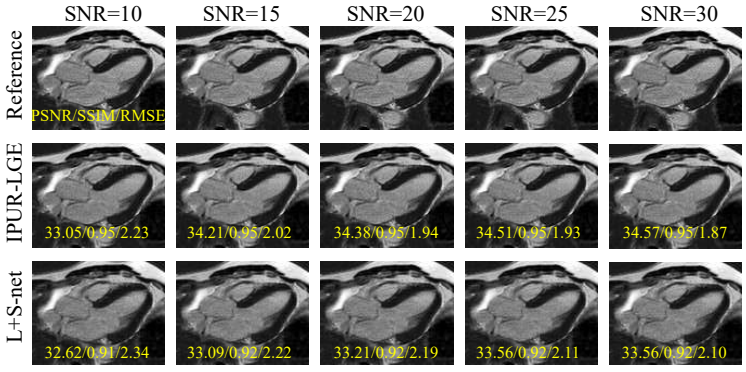

Fig. 4. Robustness evaluation for a 53-year-old healthy volunteer under varying SNR (10–30 dB) at $R = 11.5$. Metrics (PSNR, SSIM, and RMSE) are annotated on the images. Note: The RMSE values are scaled by a factor of 100 for better visualization.

Table 2. Average quantitative performance (PSNR, SSIM, RMSE) on reconstructed PSIR images across different views in the ablation studies.

		PSNR	SSIM	RMSE
2ch	**IPUR-LGE**	**39.8 ± 3.8**	**0.9595 ± 0.0196**	**0.0166 ± 0.0048**
	w/o inception	32.5 ± 4.2	0.9198 ± 0.0344	0.0256 ± 0.0135
	w/o LGE	33.7 ± 4.4	0.9445 ± 0.0251	0.0253 ± 0.0124
3ch	**IPUR-LGE**	**35.2 ± 3.2**	**0.9578 ± 0.0192**	**0.0186 ± 0.0073**
	w/o inception	33.3 ± 3.2	0.9408 ± 0.0297	0.0228 ± 0.0086
	w/o LGE	34.1 ± 4.0	0.9529 ± 0.0224	0.0211 ± 0.0083
4ch	**IPUR-LGE**	**36.2 ± 3.5**	**0.9521 ± 0.0215**	**0.0132 ± 0.0047**
	w/o inception	33.7 ± 2.8	0.9386 ± 0.0344	0.0211 ± 0.0066
	w/o LGE	34.2 ± 3.2	0.9428 ± 0.0324	0.0207 ± 0.0072
sax	**IPUR-LGE**	**40.1 ± 2.4**	**0.9562 ± 0.0152**	**0.0104 ± 0.0031**
	w/o inception	35.4 ± 3.1	0.9303 ± 0.0228	0.0178 ± 0.0063
	w/o LGE	37.8 ± 3.9	0.9498 ± 0.0255	0.0146 ± 0.0062

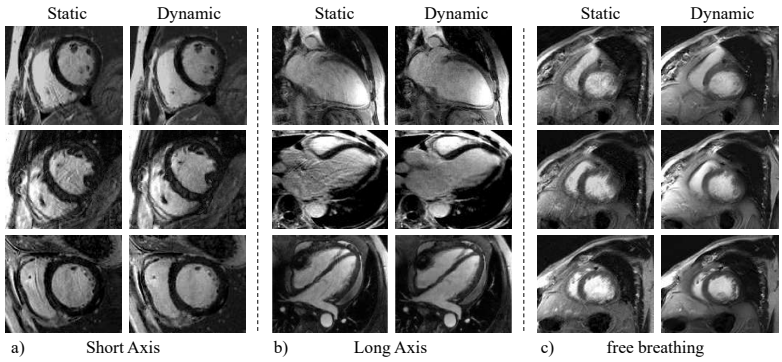

Fig. 5. Comparison between IPUR-LGE and clinical static LGE. a) Short-axis ($R = 12.5$) and b) long-axis views ($R = 11.2 - 14.8$). c) Free-breathing reconstructions ($R = 12.5$) of three short-axis slices from a 58-year-old male with coronary heart disease.

Fig.4 shows the robustness analysis results of IPUR-LGE and L+S-Net methods on noise. With an acceleration factor of R = 11.5, L+S-Net exhibited visible residual artifacts even at 30 dB. Conversely, IPUR-LGE consistently maintained clean backgrounds and sharp structural edges across all SNR range. Quantitative results also demonstrate that IPUR-LGE outperforms L+S-Net across all noise levels and exhibits robust stability against noise interference.

Fig. 5 shows the comparison results of IPUR-LGE against the standard clinical single-frame static LGE imaging. Under high acceleration factors, conventional static imaging suffers from significant aliasing artifacts and edge blurring (see Fig. 5 a) and b)). Furthermore, under challenging free-breathing conditions (Fig. 5 c)), the static LGE images exhibited severe respiratory motion artifacts. In contrast, IPUR-LGE effectively mitigates motion-induced blurring, yielding robust reconstructions with clear myocardial anatomy.

5 Discussion and Conclusion

In this study, we reformulated segmented PSIR-LGE reconstruction as a frame-resolved dynamic multi-frame reconstruction problem. IPUR-LGE integrated an inception-powered regularizer with a memory-efficient fixed-point equilibrium model. This architectural design adaptively expands the receptive field to disentangle critical myocardial textures from severe aliasing artifacts, effectively breaking the trade-off between noise amplification and over-smoothing that typically limits baselines like MoDL and Learned_DC. Furthermore, including LGE samples in the mixed-modality training set contributes to better preservation of LGE-related image characteristics. Validated on extensive 3T and 5T clinical cohorts, including challenging free-breathing scenarios, IPUR-LGE achieves robust reconstruction with improved artifact suppression and myocardial structure preservation. By consistently outperforming static standards and unrolling methods, IPUR-LGE demonstrates promising potential for accelerated clinical LGE reconstruction. Future work will expand validations on ultra-high-field 5T systems and incorporate blinded radiological scoring to further translate this dynamic multi-frame approach into routine clinical practice.

Acknowledgments. This work was supported in part by the National Natural Science Foundation of China under grant nos. 62322119, 62125111, 62331028, and 62531024; in part by the National Key R&D Program of China under grant nos. 2021YFF0501402, 2021YFF0501503, and 2023YFA1011403; and in part by the Guangdong Basic and Applied Basic Research Foundation under grant no. 2025A1515012966.

Disclosure of Interests. The authors have no competing interests to declare that are relevant to the content of this article.

References

1. Aggarwal, H.K., Mani, M.P., Jacob, M.: MoDL: Model-based deep learning architecture for inverse problems. IEEE Transactions on Medical Imaging **38**(2), 394–405 (2019). https://doi.org/10.1109/TMI.2018.2865356
2. Bai, S., Kolter, J.Z., Koltun, V.: Deep equilibrium models. In: Advances in Neural Information Processing Systems (NeurIPS). vol. 32 (2019)
3. Bustin, A., Fuin, N., Botnar, R.M., et al.: From compressed-sensing to artificial intelligence-based cardiac MRI reconstruction. Frontiers in Cardiovascular Medicine **7**, 17 (2020). https://doi.org/10.3389/fcvm.2020.00017
4. Cheng, J., Cui, Z.X., Huang, W., et al.: Learning data consistency and its application to dynamic MR imaging. IEEE Transactions on Medical Imaging **40**(11), 3140–3153 (2021). https://doi.org/10.1109/TMI.2021.3083057
5. Coleman, G.C., Shaw, P.W., Balfour, P.C., et al.: Prognostic value of myocardial scarring on CMR in patients with cardiac sarcoidosis. JACC: Cardiovascular Imaging **10**(4), 411–420 (2017). https://doi.org/10.1016/j.jcmg.2016.05.009
6. Feng, L., Grimm, R., Block, K.T., et al.: XD-GRASP: Golden-angle radial MRI with reconstruction of extra motion-state dimensions using compressed sensing. Magnetic Resonance in Medicine **75**(2), 775–788 (2016). https://doi.org/10.1002/mrm.25665

7. Fotaki, A., Pushparajah, K., Rush, C., et al.: Highly efficient free-breathing 3D whole-heart imaging in 3-min: Single center study in adults with congenital heart disease. Journal of Cardiovascular Magnetic Resonance **26**(1), 100008 (2024). https://doi.org/10.1016/j.jocmr.2023.100008
8. Griswold, M.A., Jakob, P.M., Heidemann, R.M., et al.: Generalized autocalibrating partially parallel acquisitions (GRAPPA). Magnetic Resonance in Medicine **47**(6), 1202–1210 (2002). https://doi.org/10.1002/mrm.10171
9. Hammernik, K., Klatzer, T., Kobler, E., et al.: Learning a variational network for reconstruction of accelerated MRI data. Magnetic Resonance in Medicine **79**(6), 3055–3071 (2018). https://doi.org/10.1002/mrm.26977
10. Huang, W., Ke, Z., Cui, Z.X., et al.: Deep low-rank plus sparse network for dynamic MR imaging. Medical Image Analysis **73**, 102190 (2021). https://doi.org/10.1016/j.media.2021.102190
11. Kellman, P., Arai, A.E., McVeigh, E.R., et al.: Phase-sensitive inversion recovery for detecting myocardial infarction using gadolinium-delayed hyperenhancement. Magnetic Resonance in Medicine **47**(2), 372–383 (2002). https://doi.org/10.1002/mrm.10051
12. Luo, C., Zhou, T., Cui, Z.X., et al.: Matrix completion-informed deep unfolded equilibrium models for self-supervised k-space interpolation in MRI. Medical Physics (2025). https://doi.org/10.1002/mp.17924
13. Lustig, M., Donoho, D., Pauly, J.M.: Sparse MRI: The application of compressed sensing for rapid MR imaging. Magnetic Resonance in Medicine **58**(6), 1182–1195 (2007). https://doi.org/10.1002/mrm.21391
14. Munoz, C., Bustin, A., Neji, R., et al.: Motion-corrected 3D whole-heart water-fat high-resolution late gadolinium enhancement cardiovascular magnetic resonance imaging. Journal of Cardiovascular Magnetic Resonance **22**, 53 (2020). https://doi.org/10.1186/s12968-020-00649-5
15. Parikh, N., Boyd, S.: Proximal algorithms. Foundations and Trends in Optimization **1**(3), 127–239 (2014). https://doi.org/10.1561/2400000003
16. Phair, A., Botnar, R.M., Prieto, C.: Reconstruction techniques for accelerating dynamic cardiac MRI. Journal of Cardiovascular Magnetic Resonance **27**(1), 101095 (2025). https://doi.org/10.1016/j.jocmr.2025.101095
17. Pruessmann, K.P., Weiger, M., Scheidegger, M.B., Boesiger, P.: Sense: sensitivity encoding for fast mri. Magnetic Resonance in Medicine **42**(5), 952–962 (1999). https://doi.org/10.1002/(SICI)1522-2594(199911)42:5<952::AID-MRM16>3.0.CO;2-S
18. Qin, C., Schlemper, J., Caballero, J., et al.: Convolutional recurrent neural networks for dynamic MR image reconstruction. IEEE Transactions on Medical Imaging **38**(1), 280–290 (2018). https://doi.org/10.1109/TMI.2018.2863670
19. Rich, A., Gregg, M., Jin, N., et al.: CAVA: Cartesian sampling with variable density and adjustable temporal resolution. Magnetic Resonance in Medicine **83**(6), 2015–2025 (2020). https://doi.org/10.1002/mrm.28059
20. Sandino, C.M., Cheng, J.Y., Chen, F., et al.: Accelerating cardiac cine MRI using a deep learning-based ESPIRiT reconstruction. Magnetic Resonance in Medicine **85**(1), 152–167 (2021). https://doi.org/10.1002/mrm.28420
21. Simonyan, K., Zisserman, A.: Very deep convolutional networks for large-scale image recognition. In: International Conference on Learning Representations (ICLR) (2015)
22. Wang, S., Wu, R., Jia, S., et al.: Knowledge-driven deep learning for fast MR imaging: Undersampled MR image reconstruction from supervised to un-

supervised learning. Magnetic Resonance in Medicine **92**(2), 496–518 (2024). https://doi.org/10.1002/mrm.30105
23. Weingartner, S., Demirel, O.B., Shenoy, C., et al.: Functional LGE imaging: Cardiac phase-resolved assessment of focal fibrosis. In: IEEE Engineering in Medicine and Biology Society (EMBC). pp. 1207–1210 (2019). https://doi.org/10.1109/EMBC.2019.8856722
24. Xue, H., Greiser, A., Zuehlsdorff, S., et al.: Phase-sensitive inversion recovery for myocardial T1 mapping with motion correction and parametric fitting. Magnetic Resonance in Medicine **69**(5), 1408–1420 (2013). https://doi.org/10.1002/mrm.24385
25. Yu, W., Luo, M., Zhou, P., et al.: InceptionNeXt: When inception meets ConvNeXt. In: IEEE/CVF Conference on Computer Vision and Pattern Recognition (CVPR). pp. 5672–5683 (2024)
26. Zeilinger, M.G., Kunze, K.P., Munoz, C., et al.: Non-rigid motion-corrected free-breathing 3D myocardial Dixon LGE imaging in a clinical setting. European Radiology **32**, 4340–4351 (2022). https://doi.org/10.1007/s00330-022-08560-6
27. Zhou, T., Shang, K., Liu, C., et al.: Deep equilibrium–adversarial robust unfolding network for MRI reconstruction. Medical Physics (2025). https://doi.org/10.1002/mp.70185